Atmos. Chem. Phys. Discuss., https://doi.org/10.5194/acp-2018-1123
Manuscript under review for journal Atmos. Chem. Phys.
Discussion started: 23 November 2018

Atmospheric Chemistry and Physics Discussions

Reactive nitrogen (NO_y) and ozone responses to energetic electron precipitation during Southern Hemisphere winter

Pavle Arsenovic[1,*], Alessandro Damiani[2], Eugene Rozanov[1,3,4], Bernd Funke[5], Andrea Stenke[1], Thomas Peter[1]

[1]Institute for Atmospheric and Climate Science ETH, Zürich, Switzerland
[2]Center for Environmental Remote Sensing (CEReS), Chiba University, Chiba, Japan
[3]Physikalisch-Meteorologisches Observatorium Davos – World Radiation Center, Davos, Switzerland
[4]Pushkov Institute of Terrestrial Magnetism, Ionosphere, and Radio Wave Propagation, Russian Academy of Sciences, Kaliningrad, Russia
[5]Instituto de Astrofisica de Andalucía, CSIC, Granada, Spain
[*]Now at Empa, Dübendorf, Switzerland

Correspondence to: Pavle Arsenovic (pavle.arsenovich@gmail.com)

Abstract. Energetic particle precipitation (EPP) affects the chemistry of the polar middle atmosphere by producing reactive nitrogen (NO_y) and hydrogen (HO_x) species, which then catalytically destroy ozone. Recently, there have been major advances in constraining these particle impacts through a parametrization based on high quality observations. Here we investigate the effects of low (auroral) and middle (radiation belt) energy range electrons, separately and in combination, on reactive nitrogen and hydrogen species as well as on ozone during Southern Hemisphere winters from 2002 to 2010 using the chemistry-climate model SOCOL3-MPIOM. Our results show that, in absence of solar proton events, low energy electrons produce the majority of NO_y in the polar mesosphere and stratosphere. In the polar vortex, NO_y subsides and affects ozone at lower altitudes, down to 10 hPa. Comparing a year with high electron precipitation with a quiescent period, we found large ozone depletion in the mesosphere; as the anomaly propagates downward, 15 % less ozone is found in the stratosphere during winter, which is confirmed by satellite observations. Only with both low and middle energy electrons, our model reproduces the observed stratospheric ozone anomaly.

1 Introduction

Energetic particles originating from the Sun, the magnetosphere, or from outside the solar system continuously precipitate into the Earth's atmosphere and can influence atmospheric processes. They ionize neutral air molecules especially in the middle and upper polar atmosphere and create odd nitrogen and hydrogen species, NO_x ([N] + [NO] + [NO_2]) and HO_x ([H] + [OH] + [HO_2]). NO_x and HO_x radicals can catalytically deplete ozone. The *in-situ* destruction of ozone in the mesosphere is characteristic for HO_x due to its fast reaction rates (Bates and Nicolet 1950). On the other hand, NO_x, in the absence of sunlight, subsides within the down-welling branch of the overturning circulation, affecting ozone concentrations at lower altitudes (Solomon *et al* 1982).

High energy particles, i.e. solar protons (Jackman *et al* 2008) and radiation belt electrons (Semeniuk *et al* 2011, Arsenovic *et al* 2016) can penetrate directly into the mesosphere and stratosphere. Electrons of lower energies (< 30 keV, auroral) originate from the magnetosphere as well as the radiation belt electrons (Mironova *et al* 2015), but they get accelerated in the magnetotail and precipitate into the lower thermosphere in the auroral ovals (55 – 70° geomagnetic latitude) (Baker *et al* 2001, Barth *et al* 2003).

There have been numerous attempts to include low energy electrons (LEE) in climate models. Chemistry-climate models with top in the thermosphere, e.g. HAMMONIA (Schmidt *et al* 2006), KASIMA (Reddmann *et al* 2010) and WACCM (Marsh *et al* 2007, Andersson *et al* 2018), have included effects of LEE directly because they deposit their energy within the model domain. For climate models that have an upper lid below the thermosphere, a prescription of LEE as NO_x influx through the model top is recommended (Matthes *et al* 2017). Baumgaertner *et al* (2009) has developed a parameterization of this flux based on the geomagnetic activity A_p index, a daily worldwide measure of the effects of solar wind on the Earth magnetic field. When incorporated into several chemistry-climate models, results showed significant ozone depletion in the mesosphere and stratosphere (Baumgaertner *et al* 2011). For the SOCOL chemistry-climate model Rozanov *et al* (2012) also found a significant ozone decreases in the mesosphere and stratosphere, with peak values around 10 % in September around 36 km altitude over the Antarctic.

Funke *et al* (2016) have recently developed a semi-empirical model that calculates concentrations and fluxes of mesospheric and stratospheric NO_y compounds ($[NO] + [NO_2] + 2\times [N_2O_5] + [HNO_3] + [ClONO_2]$) based on the Michelson Interferometer for Passive Atmospheric Sounding (MIPAS) observations. The model exploits the nearly linear relationship in the mesosphere between A_p index with observed NO_y produced by EPP. This advance in the representation of LEE in climate models motivates us to investigate if LEE can have a larger impact on atmospheric chemistry than previously thought. Moreover, this LEE parameterization is a part of the recommended solar forcing dataset for climate models within the upcoming Coupled Model Intercomparison Project Phase 6 (CMIP-6, Matthes *et al* 2017). It is therefore important to demonstrate that the particle impact is well represented in chemistry-climate models.

It is crucial to have a realistic representation of EPP in models as the introduced signal impacts atmospheric chemistry and potentially regional climate (Baumgaertner *et al* 2011, Rozanov *et al* 2012, Seppälä *et al* 2013, Maliniemi *et al* 2014). Here we present results from a state of the art chemistry-climate model that employs the new Funke *et al* (2016) parameterization of LEE together with the previous representations of other energetic particles. We compare our results with the satellite observations. This paper focuses on evaluating NO_x and ozone response to LEE precipitation in Antarctic winters (JJA: June, July and August), in order to avoid the more complicated Arctic polar vortex with its high variability and strong dependence on meteorological conditions (Hitchcock *et al* 2013).

Atmos. Chem. Phys. Discuss., https://doi.org/10.5194/acp-2018-1123
Manuscript under review for journal Atmos. Chem. Phys.
Discussion started: 23 November 2018

2 Methods

We used the coupled chemistry-climate model SOCOL3-MPIOM (Stenke *et al* 2013, Muthers *et al* 2014). The atmospheric dynamic component of the model is ECHAM5.4 (Roeckner and Bäuml 2003), coupled to the air chemistry module MEZON (Rozanov *et al* 1999, Egorova *et al* 2003) and the interactive ocean module MPIOM (Marsland *et al* 2002, Jungclaus *et al* 2006). We carried out the experiments with T31 spectral resolution on 39 vertical levels from the surface up to 0.01 hPa.

The model boundary conditions and parameterizations are identical to those described in Arsenovic *et al* (2016), except for the LEE parameterization. Following Calisto *et al* (2011), galactic cosmic rays (GCR) are parameterized as a function of geomagnetic latitude, pressure and solar modulation potential. Ionization by solar protons (SP) is treated according to Jackman *et al* (2008) and middle energy electrons (MEE) with energies between 30 and 300 keV are taken from the Atmospheric Ionization Module Osnabrück (AIMOS) v1.6 (Wissing and Kallenrode 2009, Arsenovic *et al* 2016). Electrons of energies higher than 300 keV are not included in the model due to a lack of adequate parameterization.

For LEE, we are using the semi-empirical model for NO_y influx by Funke *et al* (2016) through the model top. As more than 99 % of the NO_y at this altitude is in the form of nitrogen monoxide, NO (Brasseur and Solomon 2005), we approximate the NO_y influx calculated by the semi-empirical model as NO influx at this level in SOCOL3-MPIOM. Matthes *et al* (2017) also implemented the parameterization by Funke *et al* (2016) in the EMAC model. They used a different approach, prescribing NO concentrations (instead of fluxes) in the model within the 0.09 - 0.01 hPa layer and performed the simulations with specified dynamics. Prescribing concentrations requires overwriting NO values during the model run and might be inconsistent with modeled background atmospheric state and the treatment of the physical and chemical processes in the model. This is not the case for influx approach and therefore we prescribe the NO influx instead of mixing ratios.

Figure 1 shows the monthly mean geomagnetic A_p index that covers our simulated period. Period 2002-2005 was characterized by a rather high A_p index and the 2006-2010 period by low values. For our simulations, we have used daily NO fluxes calculated from daily A_p indices.

Four sets of 6-member ensemble simulations were carried out, covering the 2002-2010 period: the "ALL" simulation, that includes all energetic particles (GCR, SP, MEE and LEE), the "LEE" simulation (GCR, SP and LEE), the "MEE" simulation (GCR, SP and MEE) and the reference, "REF" simulation (GCR and SP). All these simulations have the same model boundary conditions and differ only in the inclusion of the low/middle energy electron precipitation.

We used two satellite datasets to evaluate our model results: MIPAS for nitrogen species and the Microwave Limb Sounder (MLS) for ozone. MIPAS was a Fourier transform spectrometer aboard the ENVISAT satellite (Fischer *et al* 2008). The quality of MIPAS NO_y and individual NO_y species has been extensively assessed in SPARC (2017), as well as specific validation studies (e.g. Bender *et al* 2015; Sheese *et al* 2016). Since it provides the entire NO_y budget in the upper atmosphere (on 27 pressure levels between 100 and 0.01 hPa), we used this dataset to validate simulated NO_y. The MLS aboard Aura satellite (Waters *et al* 2006) provided daily measurements of ozone profiles (Froidevaux *et al* 2008) in the middle and upper atmosphere

since August 2004. We used MLS observations to evaluate modeled ozone. The vertical resolution of MLS O_3 (v4.2) is about 3 km in the stratosphere, increasing up to about 5 km in the mesosphere (Livesey *et al* 2018).

3 Results

3.1 NO_y enhancement propagation

Figure 2 shows the difference in NO_y concentration between the geomagnetically active year 2005 and the mean over the geomagnetically quiescent period 2006 – 2010 averaged over 70 – 90°S. The MIPAS observations (Figure 2a) show a NO_y enhancement throughout the mesosphere and upper stratosphere. In terms of mixing ratio, the highest increase of 500 – 600 ppbv is found in the upper mesosphere around 0.01 hPa (~80 km). There, the highest monthly values are observed in June. In the following months, this anomaly descends and reaches lower levels. In July, the NO_y enhancement of around 10 ppbv reaches the upper stratosphere around 2 hPa, and the increase, although smaller, is visible all the way down to 10 hPa. In the following months, the MIPAS nominal data were unavailable due special observation mode campaigns.

The ALL experiment (Figure 2b) shows a very similar pattern of NO_y as the observations. The NO_y increase of 500 – 600 ppbv in the upper mesosphere around 0.01 hPa is similar as in MIPAS. However, the wintertime NO_y peak below is slightly overestimated in the model compared to MIPAS. This is particularly visible in the lower mesosphere in June, as the modeled 100 ppbv NO_y enhancement reaches 0.1 hPa. The mesospheric anomaly extends into the stratosphere, but remains confined to the upper stratosphere, above 10 hPa, as in observations. The modeled NO_y overestimation suggests that downward transport is somewhat too fast in the model, or the photochemical lifetime of NO_y is too long, or horizontal mixing with mid-latitudes is underestimated. The modeled NO_y enhancement in September stems from a SP event (NOAA, 2018). In contradiction to our results, the EMAC model slightly underestimates NO_y even during polar summer, for two pressure levels, 0.1 and 1 hPa (Matthes *et al* 2017). Sinnhuber *et al* (2018) compared NO_y observed by MIPAS with the results of 3dCTM, KASIMA and EMAC chemistry-climate models and also showed overestimation of modeled NO_y in the southern hemisphere.

The LEE simulation (Figure 2c) shows very similar anomalies as ALL. The largest differences are in the upper mesosphere, where LEE anomalies reach around 400 ppbv, which is underestimated compared to 500-600 ppbv found in MIPAS and ALL. A second interesting difference compared to ALL is the SP event in September. In LEE simulation, it reaches around 60 ppbv, while in ALL it exceeds 100 ppbv. This difference is coming from increased MEE precipitation that coincided with the SP event (see Arsenovic *et al* 2016, Figure 1a).

The MEE simulation (Figure 2d) is drastically different from MIPAS as well as the ALL and LEE simulations. Although NO_y enhancement in the modeled geomagnetically active year exists, it is significantly decreased compared with the previous results. The pronounced modeled NO_y anomaly maximum from the mesosphere is absent and enhancement of 10 ppbv does not reach the stratosphere. Nevertheless, although less intense, increased NO_y is present throughout the mesosphere and stratosphere, and the NO_y increase in September due to the SP event exceeds again 100 ppbv, as in the ALL simulation.

The reference run in Figure 2e shows NO_y increase due to the SP events in the year 2005. In this year, there were 6 observed SP events in the shown timeframe – May 14, June 16, July 14 and 27, August 22 and September 8 (NOAA, 2018). In the geomagnetically inactive period, 2006-2010, there were no observed SP events in the presented months. Therefore, by excluding electron precipitation, the SP events only cannot reproduce the observed features.

From the presented, we conclude that inclusion of only LEE was sufficient to reproduce most of the NO_y enhancements. The MEE contribution to NO_y increases is minor and brings model closer to observations mainly in the upper mesosphere. As SP events can have impact on precipitation from outer Van Allen belt (Pierrard and Lopez Rosson 2016), MEE precipitation could significantly contribute to NO_y increases in such events.

3.2 O_3 anomaly propagation

In study of Matthes *et al* (2017), ozone responses were evaluated by comparing high and low geomagnetic activity years and not by on/off experiments as done here and their estimate shows good agreement with satellite observations (Fytterer *et al* 2015). To evaluate our simulated ozone responses, we follow a similar approach as used in Matthes *et al* (2017), that is, we compared our simulations with observations from MLS. We analyzed 2005 – 2010 period when both, simulation and MLS data, are available.

Ozone anomalies from MLS observations during the high geomagnetically active year are depicted in Figure 3a. They are calculated as the difference averaged over 70 – 90^0 S between the active year (2005) and the average of geomagnetically quiescent years (2006 – 2010) divided by the ozone averaged over the whole period (2005 – 2010). Observations show around 20 % less ozone in the upper mesosphere (< 0.1 hPa) occurring mostly in JJA period. The exception is the SP event on September 8, 2005. It created an ozone anomaly of up to 80 % stretching throughout whole mesosphere. The mesosphere below 0.1 hPa shows a little difference between the geomagnetically active and quiescent years in absence of SP events. The observed negative ozone anomaly appears again around the stratopause in late June and propagates downwards to nearly 10 hPa in early September. The peak ozone anomaly occurs in August around 3 hPa, reaching ~15 %. Our results agree with the results from previous modeling studies (Rozanov *et al* 2012, Reddmann *et al* 2010) and observations (Damiani *et al* 2016, Fytterer *et al* 2015).

The ALL simulation (Figure 3b) shows a negative ozone anomaly in the mesosphere as well. However, the magnitude is generally higher (around 30 %) and it is present from May to September. The September 2005 SP event is visible in the model simulations as well and descends from around 1 hPa in late September, reaching 10 hPa in late October. A similar pattern, but less obvious, is seen in the observations. Ozone anomalies in the lower mesosphere (0.5 – 0.1 hPa) are more pronounced in the model than in MLS observations. This is particularly evident in June when the modeled upper-mesosphere anomaly appears to relate to the upper-stratospheric anomaly, in contrast to the observations. This suggest that HO_x production by MEE might be overestimated. In the upper stratosphere model simulations agree well with observations. The decrease propagates downwards, reaching approximately 10 hPa in August, with a peak around 15 % in good agreement with the observations.

Ozone anomalies in the LEE simulation are shown in Figure 3c. Negative ozone anomalies are present mostly in the upper mesosphere (above 0.3 hPa) and have similar magnitude to ALL. Although in the LEE simulation mesospheric ozone anomaly is overestimated compared to MLS observations, the stratospheric anomaly is almost completely absent. This is surprising, as there are very similar NO_y anomalies in the ALL and LEE simulations (see Figure 2).

Our MEE simulation shows similar ozone anomalies to LEE (Figure 3d). The anomalies are confined to a region above 1 hPa and are somewhat reduced compared to LEE and ALL. Similar to LEE, the stratospheric ozone anomaly seen in the observations and ALL simulation is almost absent.

In REF simulation (Figure 3e) most of the ozone anomaly features seen in observations and ALL are missing. The only depletion of ozone in this simulation is caused by SP events in the year 2005. Most of the observed events (May 14, June 16, July 14 and 27, August 22 and September 8) are clearly visible.

Recent study based on CCM WACCM (Andersson *et al* 2018) showed ozone anomaly propagation differences between high-A_p and low-A_p winters in the Southern Hemisphere. Their results are comparable with our ALL and LEE simulations. Compared with our ALL simulation, their ozone anomaly in case of all EEP of around 7 % is lower and occurs later (in October as opposed to August). However, their LEE simulation does not show significant ozone anomaly in the stratosphere, which is also the case in our results.

3.3 EEP effect on NO_y, HO_x and O_3

To estimate the total effect of energetic electron precipitation on NO_y, HO_x and ozone, we calculated the differences of experiment simulations (ALL, LEE and MEE) and REF simulation for the geomagnetically active period (2002 – 2005) using the simulated monthly values. Note that this is an idealized comparison and it is not directly comparable with observations, as there is always some amount of particle precipitation in the atmosphere (Funke et al 2014), unlike in LEE, MEE and REF simulation.

The zonal mean of austral winter (JJA) average NO_y differences between ALL and REF is shown in Figure 4a. In polar night, NO_y is transported to lower altitudes by descending air motion. Significant modeled NO_y enhancements are present in the whole mesosphere and upper stratosphere above 10 hPa. Around 0.01 hPa, EPP produced NO_y increases from 50 ppbv at around 60° S to more than 500 ppbv at the pole. The differences in HO_x between those two experiments are shown on Figure 4b. Increases are mostly confined to the upper mesosphere and they reach the maximum of around 5 ppbv. However, smaller (< 1ppbv) but statistically significant HO_x increase appears in lower mesosphere and upper stratosphere around 60° S. Increases of NO_y and HO_x impact the ozone chemistry. Figure 4c shows changes in ozone concentrations due to electron precipitation. Ozone is significantly reduced throughout the whole polar region above 10 hPa. There are two peaks of ozone anomaly. The maximum decrease of up to 65 % (350 – 400 ppbv) is located in the upper mesosphere. This decrease is more severe than in previous modeling studies (Rozanov et al 2012), but this is because we focus on the geomagnetically active winters, when EPP effects are much more pronounced. The magnitude of ozone depletion is gradually decreasing with height reaching ~15 %

(>200 ppbv) at the stratopause. The second ozone depletion peak is located between 10 and 1 hPa, reaching 15 % (>400 ppbv). A similar ozone response as in ALL has been shown by Semeniuk et al. (2011).

Figure 4d shows the difference between modeled NO_y in LEE and REF simulation. Similarly, as in Figure 2, modeled NO_y in LEE simulation is very similar as in ALL, confirming the fact that the most of the NO_y is coming from LEE. Slight reduction to ALL still exists, visible mostly at 0.1 hPa at 90° S. Here, the value of NO_y is 100 ppbv while it is somewhat more in Figure 4a. Second difference is the absence of the enhancement equatorward of 30° S which is present in Figure 4a. Increase of HO_x in case of LEE is illustrated on Figure 4e. Changes of HO_x are very small and statistically insignificant, except for small (<1 ppbv) increase in the polar upper mesosphere. This is expected as LEE do not produce HO_x. The small increase could be explained by increase of NO_y which causes small increase of background HO_x through the Verronen and Lehmann (2015) mechanism. As Verronen and Lehmann (2015) pointed out, enhanced NO coming from EEP leads to HO_x repartitioning increasing HO_x concentrations. Figure 4f shows ozone changes due to the LEE. Similar ozone decrease pattern as in Figure 4c exists but with a reduced intensity. The upper-mesospheric reduction reaches 35 % (~200 ppbv) and the upper-stratospheric anomaly is halved compared to ALL (200 ppbv ≙ 10 %). The absence of HO_x increases and reduced ozone anomalies compared to ALL illustrates the importance of MEE.

Figure 4g shows increase of NO_y due to the MEE. Although MEE cause increase of NO_y, modeled NO_y is significantly reduced in the whole area compared to LEE and ALL simulation. In the upper mesosphere, this increase is around 50 ppbv, or tenth of total produced NO_y in ALL simulation. Equatorward from 30° S NO_y enhancement is present again, as in ALL simulation. This enhancement is coming from the fact that MEE do not necessarily precipitate inside the polar vortex, as they precipitate in the sub-auroral ovals, which are centered around the geomagnetic pole. In contrast, NO_y coming from LEE descends into the mesosphere in the down-welling air motion inside of the polar vortex. The sum of NO_y increases (not shown) due to the LEE (Fig 4d) and due to the MEE (Fig 4g) closely reassembles NO_y increase as in ALL case (Fig 4a).

Increases of HO_x due to MEE are presented in Figure 4h. Enhancements are present mostly in the upper mesosphere reaching 4 ppbv. The position and intensity of HO_x is very similar to ALL, but somewhat reduced. Because MEE produce OH, neglecting MEE in climate models would lead to an underestimation of HO_x; neglecting LEE would also lead to an underestimation of HO_x through the changed HO_x partitioning (Verronen and Lehmann, 2015). Changes in ozone concentrations due to MEE are shown in Figure 4i. Negative ozone anomalies are present in the mesosphere and in the upper stratosphere, albeit stratospheric anomaly is statistically not significant. Biggest reduction with 35 % (~200 ppbv) is visible in the upper mesosphere. The anomaly in the upper stratosphere (10 – 1 hPa) does not exceed 100 ppbv. Interestingly, summing stratospheric ozone anomaly from LEE (Fig 3f) and from MEE (Fig 3i) does not reproduce ALL ozone anomaly (Fig 3c). The sum of the LEE and MEE ozone anomaly accounts for around 300, while ALL shows about 400 ppbv between 10 and 1 hPa. Since sum of enhanced NO_y due to LEE and MEE corresponds to ALL NO_y and HO_x enhancements occur in mesosphere, this discrepancy in ozone anomaly cannot be chemically explained. It could be caused by changes in dynamics (polar vortex strength) and temperature (which affects reaction rates).

Our results indicate that LEE and MEE are equally responsible for ozone anomaly in the mesosphere. LEE deplete ozone through the production of large amounts of NO_y, while MEE contribute to the anomaly mostly through production of HO_x, which is more efficient ozone destructor (Brasseur and Solomon 2005). Both LEE and MEE produce stratospheric anomaly; however, LEE, through production of large amounts of NO_y are more important.

4 Conclusions

We used the period 2005-2010 comprising intervals of high and low geomagnetic activity, which is well characterized by stratospheric and mesospheric measurements of NO_y and O_3, to investigate the accuracy of representations of energetic particle forcing in a chemistry-climate model. We assessed the impact of employing a new parameterization of LEE (< 30 keV) recommended for CMIP-6 in combination with the AIMOS parameterization for MEE (30 – 300 keV) on the simulated NO_y, HO_x and ozone variability. We used the SOCOL3-MPIOM climate model and focused on the Southern Hemispheric winter season. We compared NO_y with stratospheric and mesospheric MIPAS observations. The model captures the main features very well, but shows some differences in the winter maxima. LEE can reproduce most of the NO_y features, without including MEE. However, increased MEE precipitation coincident with SP events may contribute to reproduce the observed NO_y amounts.

Simulated ozone depletion has been compared to MLS satellite observations, showing that patterns of ozone anomalies during the high EPP year 2005 compared to 2006-2010 match reasonably well. The model overestimates mesospheric ozone anomalies, but in the stratosphere a good match is accomplished. Ozone depletion of up to 15 % is found during July and August and reaches into the lower stratosphere. In essence, without including both LEE and MEE, the stratospheric anomaly cannot be accurately modeled. In addition to chemical changes, indirect changes in temperature and dynamics also play a role in the EPP-induced stratospheric ozone variation.

Most of the NO_y in the mesosphere and stratosphere is produced by LEE in the upper mesosphere and lower thermosphere (<0.01 hPa) and transported downwards. A smaller fraction, namely ~10 %, is generated in-situ by ionization due to precipitating electrons of higher energies. These electrons play an important role because they produce HO_x, which depletes ozone near HO_x source region in the mesosphere. Although not producing HO_x directly, LEE increase NO_y concentrations, which then causes repartitioning of HO_x and increase HO_x lifetime (Verronen and Lehmann 2015).

In summary, LEE and MEE lead to a reduction of ozone throughout the mesospheric and stratospheric polar region with a maximum percentage ozone depletion in the mesosphere (-65 %) and a second peak anomaly in the upper stratosphere (-15 %) with respect to the simulation where they are omitted. These chemical EPP signals can cause dynamical changes in the stratosphere that propagate into the lower atmosphere, which eventually affect regional climate (Rozanov *et al* 2012). Therefore, we recommend including both LEE and MEE in climate models.

Author contribution

PA and ER proposed the idea; PA designed and carried out the simulations and prepared the manuscript. AD analyzed MLS data and made Figure 3. BF provided MIPAS data. TP formulated the general line of research and supervised the project. All authors provided critical feedback and helped shape the research, analysis and manuscript.

Acknowledgments

This work has been supported by the Swiss National Science Foundation under Grant CRSII2-147659 (FUPSOL II). AD was supported by JST/CREST/EMS/TEEDDA fund (JPMJCR15K4) and FONDECYT (Preis 1171690). BF was supported by the Spanish MCINN (ESP2017-87143-R) and EC FEDER funds. ER was supported by the Russian Science Foundation (17-17-01060). This work is a part of ROSMIC WG1 activity within the SCOSTEP VarSITI program. The authors thank NASA Goddard Earth Science Data and Information Services Center (GES DISC) for providing Aura/MLS data (https://mls.jpl.nasa.gov/), Marina Dütsch (University of Washington) and Jelisaveta Arsenovic for assistance with improving the graphics, Amewu Mensah and William Ball (ETH, Zürich) for correcting the language.

References

Andersson, M. E., Verronen, P. T., Marsh, D. R., Seppälä, A., Päivärinta, S. M., Rodger, C. J., Clilverd, M. A., Kalakoski, N., and van de Kamp, M.: Polar Ozone Response to Energetic Particle Precipitation Over Decadal Time Scales: The Role of Medium-Energy Electrons, J. Geophys. Res. Atmos., 123 607–22, doi:10.1002/2017JD027605, 2018

Arsenovic, P., Rozanov, E., Stenke, A., Funke, B., Wissing, J. M., Mursula, K., Tummon, F., and Peter, T.: The influence of Middle Range Energy Electrons on atmospheric chemistry and regional climate, J. Atmos. Solar-Terrestrial Phys., 149, 180–90, doi:10.1016/j.jastp.2016.04.008, 2016

Baker, D. N., Barth, C. A., Mankoff, K. E., Kanekal, S. G., Bailey, S. M., Mason, G. M., and Mazur, J. E.: Relationships between precipitating auroral zone electrons and lower thermospheric nitric oxide densities: 1998–2000, J. Geophys. Res., 106, 24, 465-24, 480, doi:10.1029/2001JA000078, 2001

Barth, C. A., Mankoff, K. D., Bailey, S. M., and Solomon, S. C. 2003 Global observations of nitric oxide in the thermosphere, J. Geophys. Res. Sp. Phys., 108 1–11, doi: 10.1029/2002JA009458, 2003

Bates, D. and Nicolet, M.: The photochemistry of atmospheric water vapor, J. Geophys. Res., 301–27, doi:10.1029/JZ055i003p00301, 1950

Baumgaertner, A. J. G., Jöckel, P., and Brühl, C.: Energetic particle precipitation in ECHAM5/MESSy1 – Part 1: Downward transport of upper atmospheric NOx produced by low energy electrons, Atmos. Chem. Phys., 9, 2729-2740, doi:10.5194/acp-9-2729-2009, 2009

Baumgaertner, A. J. G., Seppälä, A., Jöckel, P., and Clilverd, M. A.: Geomagnetic activity related NO_x enhancements and polar surface air temperature variability in a chemistry climate model: modulation of the NAM index, Atmos. Chem. Phys., 11, 4521-4531, doi:10.5194/acp-11-4521-2011, 2011

Bender, S., Sinnhuber, M., Von Clarmann, T., Stiller, G., Funke, B., López-Puertas, M., Urban, J., Pérot, K., Walker, K. A., and Burrows, J. P.: Comparison of nitric oxide measurements in the mesosphere and lower thermosphere from ACE-FTS, MIPAS, SCIAMACHY, and SMR, Atmos. Meas. Tech., 8, doi:10.5194/amt-8-4171-2015, 4171–95, 2015

Brasseur, G. P. and Solomon, S.: Aeronomy of the middle atmosphere: Chemistry and physics of the stratosphere and mesosphere (Dordrect, The Netherlands: Springer), 2005

Calisto, M., Usoskin, I., Rozanov, E., and Peter, T.: Influence of Galactic Cosmic Rays on atmospheric composition and dynamics, Atmos. Chem. Phys., 11, 4547-4556, doi:10.5194/acp-11-4547-2011, 2011

Damiani, A., Funke, B., Puertas, M. L., Santee, M. L., Cordero, R. R., and Watanabe, S.: Energetic particle precipitation: A major driver of the ozone budget in the Antarctic upper stratosphere, Geophys. Res. Lett., 43, 3554–62, doi:10.1002/2016GL068279, 2016

Egorova, T., Rozanov, E., Zubov, V., and Karol, I.: Model for investigating ozone trends (MEZON), Izv. Atmos. Ocean. Phys., 39, 277–92, 2003

Fischer, H., Birk, M., Blom, C., Carli, B., Carlotti, M., von Clarmann, T., Delbouille, L., Dudhia, A., Ehhalt, D., Endemann, M., Flaud, J. M., Gessner, R., Kleinert, A., Koopman, R., Langen, J., López-Puertas, M., Mosner, P., Nett, H., Oelhaf, H., Perron, G., Remedios, J., Ridolfi, M., Stiller, G., and Zander, R.: MIPAS: an instrument for atmospheric and climate research, Atmos. Chem. Phys., 8, 2151-2188, doi:10.5194/acp-8-2151-2008, 2008

Froidevaux, L., Jiang, Y. B., Lambert, A., Livesey, N. J., Read, W. G., Waters, J. W., Browell, E. V., Hair, J. W., Avery, M. A., McGee, T. J., Twigg, L. W., Sumnicht, G. K., Jucks, K. W., Margitan, J. J., Sen, B., Stachnik, R. A., Toon, G. C., Bernath, P. F., Boone, C. D., Walker, K. A., Filipiak, M. J., Harwood, R. S., Fuller, R. A., Manney, G. L., Schwartz, M. J., Daffer, W. H., Drouin, B. J., Cofield, R. E., Cuddy, D. T., Jarnot, R. F., Knosp, B. W., Perun, V. S., Snyder, W. V., Stek, P. C., Thurstans, R. P., and Wagner, P. A.: Validation of Aura Microwave Limb Sounder stratospheric ozone measurements J. Geophys. Res. Atmos., 113, D15S20, doi/10.1029, 2008

Funke, B., López-Puertas, M., Stiller, G. P., and von Clarmann, T.: Mesospheric and stratospheric NO y produced by energetic particle precipitation during 2002-2012, J. Geophys. Res. Atmos., 119, 4429–46, doi:10.1002/2013JD021404, 2014

Funke, B., López-Puertas, M., Stiller, G. P., Versick, S., and Von Clarmann, T.: A semi-empirical model for mesospheric and stratospheric NO_y produced by energetic particle precipitation, Atmos. Chem. Phys., 16, 8667–93, doi: acp-16-8667-2016, 2016

Fytterer, T., Mlynczak, M. G., Nieder, H., Pérot, K., Sinnhuber, M., Stiller, G., and Urban, J.: Energetic particle induced intra-seasonal variability of ozone inside the Antarctic polar vortex observed in satellite data, Atmos. Chem. Phys., 15, 3327–38, doi:acp-15-3327-2015, 2015

Hitchcock, P., Shepherd, T. G., and Manney, G. L.: Statistical characterization of Arctic polar-night jet oscillation events, J. Clim., 26, 2096–116, doi:10.1175/JCLI-D-12-00202.1, 2013

Jackman, C. H., Marsh, D. R., Vitt, F. M., Garcia, R. R., Fleming, E. L., Labow, G. J., Randall, C. E., López-Puertas, M., and Funke, B.: Short- and medium-term atmospheric effects of very large solar proton events, Atmos. Chem. Phys., 8, 765-85, doi:10.5194/acp-8-765-2008, 2008

Jungclaus, J. H., Keenlyside, N., Botzet, M., Haak, H., Luo, J. J., Latif, M., Marotzke, J., Mikolajewicz, U., and Roeckner, E.: Ocean circulation and tropical variability in the coupled model ECHAM5/MPI-OM, J. Clim., 19, 3952–72, doi:10.1175/JCLI3827.1, 2006

Livesey, N. J., Read, W. G., Wagner, P. A., Froidevaux, L., Lam- bert, A., Manney, G. L., Millán, L. F., Pumphrey, Hugh, C., San- tee, M. L., Schwartz, M. J., Wang, S., Fuller, R. A., Jarnot, R. F., Knosp, B. W., and Martinez, E.: Version 4.2x Level 2 data quality and description document. Earth Observing System (EOS) Aura Microwave Limb Sounder (MLS), available at: https://mls.jpl.nasa.gov/data/v4-2_data_quality_document.pdf, last access: 10.10.2018

Maliniemi, V., Asikainen, T., and Mursula, K.: Spatial distribution of Northern Hemisphere winter temperatures during different phases, J. Geophys. Res. Atmos., 1–13, doi:10.1002/2013JD021343, 2014

Marsh, D. R., Garcia, R. R., Kinnison, D. E., Boville, B. A., Sassi, F., Solomon, S. C., and Matthes, K.: Modeling the whole atmosphere response to solar cycle changes in radiative and geomagnetic forcing, J. Geophys. Res. Atmos., 112 1–20, 10.1029/2006JD008306, 2007

Marsland, S. J., Haak, H., Jungclaus, J. H., Latif, M., and Röske, F.: The Max-Planck-Institute global ocean/sea ice model with orthogonal curvilinear coordinates, Ocean Model., 5, 91–127, doi:10.1016/S1463-5003(02)00015-X, 2002

Matthes, K., Funke, B., Andersson, M. E., Barnard, L., Beer, J., Charbonneau, P., Clilverd, M. A., Dudok De Wit, T., Haberreiter, M., Hendry, A., Jackman, C. H., Kretzschmar, M., Kruschke, T., Kunze, M., Langematz, U., Marsh, D. R., Maycock, A. C., Misios, S., Rodger, C. J., Scaife, A. A., Seppälä, A., Shangguan, M., Sinnhuber, M., Tourpali, K., Usoskin, I., Van De Kamp, M., Verronen, P. T., and Versick, S.: Solar forcing for CMIP6 (v3.2), Geosci. Model Dev., 10, 2247–302, doi:10.5194/gmd-10-2247-2017, 2017

Mironova, I. A., Aplin, K. L., Arnold, F., Bazilevskaya, G. A., Harrison, R. G., Krivolutsky, A. A., Nicoll, K. A., Rozanov, E. V., Turunen, E., and Usoskin, I. G.: Energetic Particle Influence on the Earth's Atmosphere, Space Sci. Rev., 194, 1–96, doi:10.1007/s11214-015-0185-4, 2015

Muthers, S., Anet, J. G., Stenke, A., Raible, C. C., Rozanov, E., Brönnimann, S., Peter, T., Arfeuille, F. X., Shapiro, A. I., Beer, J., Steinhilber, F., Brugnara, Y., Schmutz, W.: The coupled atmosphere-chemistry-ocean model SOCOL-MPIOM, Geosci. Model Dev., 7, 2157–79, doi:10.5194/gmd-7-2157-2014, 2014

NOAA, ftp://ftp.swpc.noaa.gov/pub/indices/SPE.txt, accessed on 10. 10. 2018

Pierrard, V. and Lopez Rosson, G.: The effects of the big storm events in the first half of 2015 on the radiation belts observed by EPT/PROBA-V, Ann. Geophys., 34 75–84, doi: 10.5194/angeo-34-75-2016, 2016

Reddmann, T., Ruhnke, R., Versick, S., and Kouker, W.: Modeling disturbed stratospheric chemistry during solar-induced NO_x enhancements observed with MIPAS/ENVISAT, J. Geophys. Res., 115, D00I11, doi:10.1029/2009JD012569, 2010

Roeckner, E. and Bäuml, G.: The Atmospheric General Circulation Model ECHAM5 Model description, Max Plank Inst., Meteorol. Sci. Rep. 1–127, 2003

Rozanov, E., Zubov, V., Schlesinger, M. E., Yang, F., and Andronova, N. G.: The UIUC three-dimensional stratospheric chemical transport model: Description and evaluation of the simulated source gases and ozone, J. Geophys. Res., 104, 11755, doi:10.1029/1999JD900138, 1999

Rozanov, E., Calisto, M., Egorova, T., Peter, T., and Schmutz, W. 2012 Influence of the Precipitating Energetic Particles on Atmospheric Chemistry and Climate, Surv. Geophys., 33, 483–501, doi:10.1007/s10712-012-9192-0, 2012

Schmidt, H., Brasseur, G. P., Charron, M., Manzini, E., Giorgetta, M. A., Diehl, T., Fomichev, V. I., Kinnison, D., Marsh, D., and Walters, S.: The HAMMONIA chemistry climate model: Sensitivity of the mesopause region to the 11-year solar cycle and CO2 doubling, J. Clim., 19, 3903–31, doi:10.1175/JCLI3829.1, 2006

Semeniuk, K., Fomichev, V. I., McConnell, J. C., Fu, C., Melo, S. M. L. L., and Usoskin, I. G.: Middle atmosphere response to the solar cycle in irradiance and ionizing particle precipitation, Atmos. Chem. Phys., 11, 5045–77, doi:10.5194/acp-11-5045-2011, 2011

Seppälä, A., Lu, H., Clilverd, M. A., and Rodger, C. J.: Geomagnetic activity signatures in wintertime stratosphere wind, temperature, and wave response, J. Geophys. Res. Atmos., 118, 2169–83, doi:10.1002/jgrd.50236, 2013

Sheese, P. E., Walker, K. A., Boone, C. D., McLinden, C. A., Bernath, P. E., Bourassa, A. E., Burrows, J. P., Degenstein, D. A., Funke, B., Fussen, D., Manney, G. L., Thomas McElroy, C., Murtagh, D., Randall, C. E., Raspollini, P., Rozanov, A., Russell, J. M., Suzuki, M., Shiotani, M., Urban, J., Von Clarmann, T., and Zawodny, J. M.: Validation of ACE-FTS version 3.5 NO_y species profiles using correlative satellite measurements, Atmos. Meas. Tech., 9, 5781–810, doi:10.5194/amt-9-5781-2016, 2016

Sinnhuber, M., Berger, U., Funke, B., Nieder, H., Reddmann, T., Stiller, G., Versick, S., von Clarmann, T., Wissing, J. M.: NO_y production, ozone loss and changes in net radiative heating due to energetic particle precipitation in 2002-2010, Atmos. Chem. Phys. 18, 1115-47, doi:10.5194/acp-18-1115-2018,2018

Solomon, S., Crutzen, P. J., and Roble, R. G.: Photochemical coupling between the thermosphere and the lower atmosphere: 1. Odd nitrogen from 50 to 120 km, J. Geophys. Res., 87, 7206, doi:10.1029/JC087iC09p07206, 1982

SPARC: The SPARC Data Initiative: Assessment of stratospheric trace gas and aerosol climatologies from satellite limb sounders. M. I. Hegglin and S. Tegtmeier (Eds.), SPARC Report No. 8, WCRP-05/2017, doi:10.3929/ethz-a-010863911, 2017

Stenke, A., Schraner, M., Rozanov, E., Egorova, T., Luo, B., and Peter, T.: The SOCOL version 3.0 chemistry-climate model: Description, evaluation, and implications from an advanced transport algorithm, Geosci. Model Dev., 6, 1407–27, doi:10.5194/gmd-6-1407-2013, 2013

Verronen, P. T. and Lehmann, R.: Enhancement of odd nitrogen modifies mesospheric ozone chemistry during polar winter, Geophys. Res. Lett., 42, 10445–52, doi:10.1002/2015GL066703, 2015

Waters, J. W., Froidevaux, L., Harwood, R. S., Jarnot, R. F., Pickett, H. M., Read, W. G., Siegel, P. H., Cofield, R. E., Filipiak, M. J., Flower, D. A., Holden, J. R., Lau, G. K., Livesey, N. J., Manney, G. L., Pumphrey, H. C., Santee, M. L., Wu, D. L., Cuddy, D. T., Lay, R. R., Loo, M. S., Perun, V. S., Schwartz, M. J., Stek, P. C., Thurstans, R. P., Boyles, M. A., Chandra, K. M., Chavez, M. C., Chen, G. S., Chudasama, B. V., Dodge, R., Fuller, R. A., Girard, M. A., Jiang, J. H., Jiang, Y., Knosp, B. W., Labelle, R. C., Lam, J. C., Lee, K. A., Miller, D., Oswald, J. E., Patel, N. C., Pukala, D. M., Quintero, O., Scaff, D. M., Van Snyder, W., Tope, M. C., Wagner, P. A., and Walch, M. J.: The Earth Observing System Microwave Limb Sounder (EOS MLS) on the aura satellite, IEEE Trans. Geosci. Remote Sens., 44, 1075–92, doi:10.1109/TGRS.2006.873771, 2006

Wissing, J. M. and Kallenrode, M. B.: Atmospheric ionization module Osnabrück (AIMOS): A 3-D model to determine atmospheric ionization by energetic charged particles from different populations, J. Geophys. Res. Sp. Phys., 114, 1–14, doi:10.1029/2009JA014419, 2009

Atmos. Chem. Phys. Discuss., https://doi.org/10.5194/acp-2018-1123
Manuscript under review for journal Atmos. Chem. Phys.
Discussion started: 23 November 2018

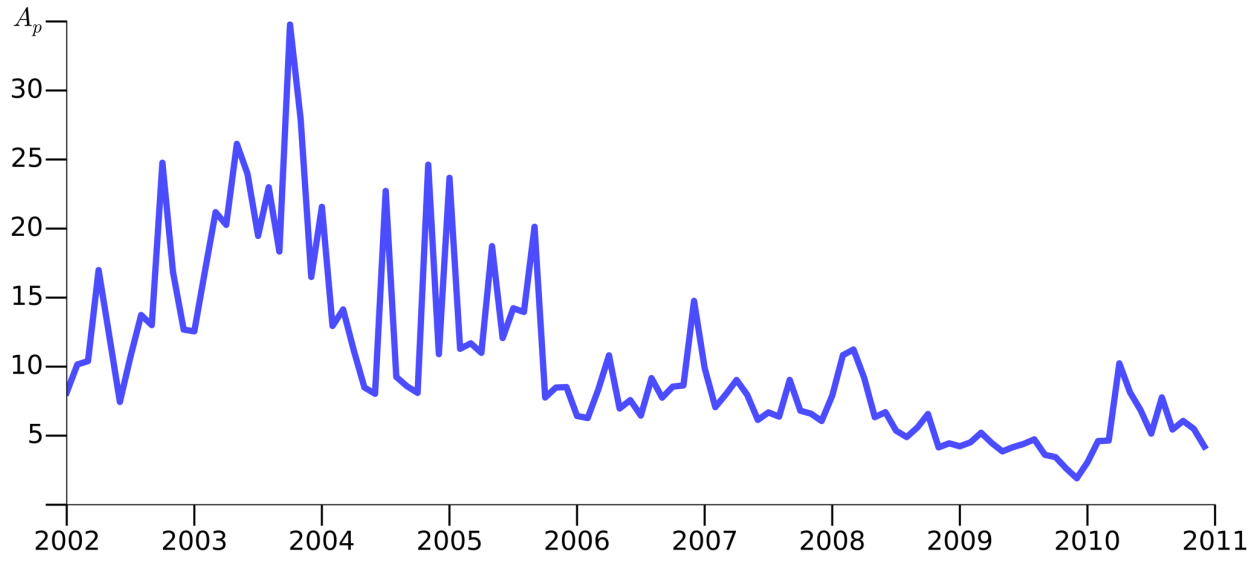

Figure 1: The monthly mean geomagnetic A_p index during the simulated period: Years 2002 – 2005 were rather active, while the period 2006 – 2010 was geomagnetically quiescent (CMIP-6 dataset; Matthes *et al* 2017).

5

Atmos. Chem. Phys. Discuss., https://doi.org/10.5194/acp-2018-1123
Manuscript under review for journal Atmos. Chem. Phys.
Discussion started: 23 November 2018

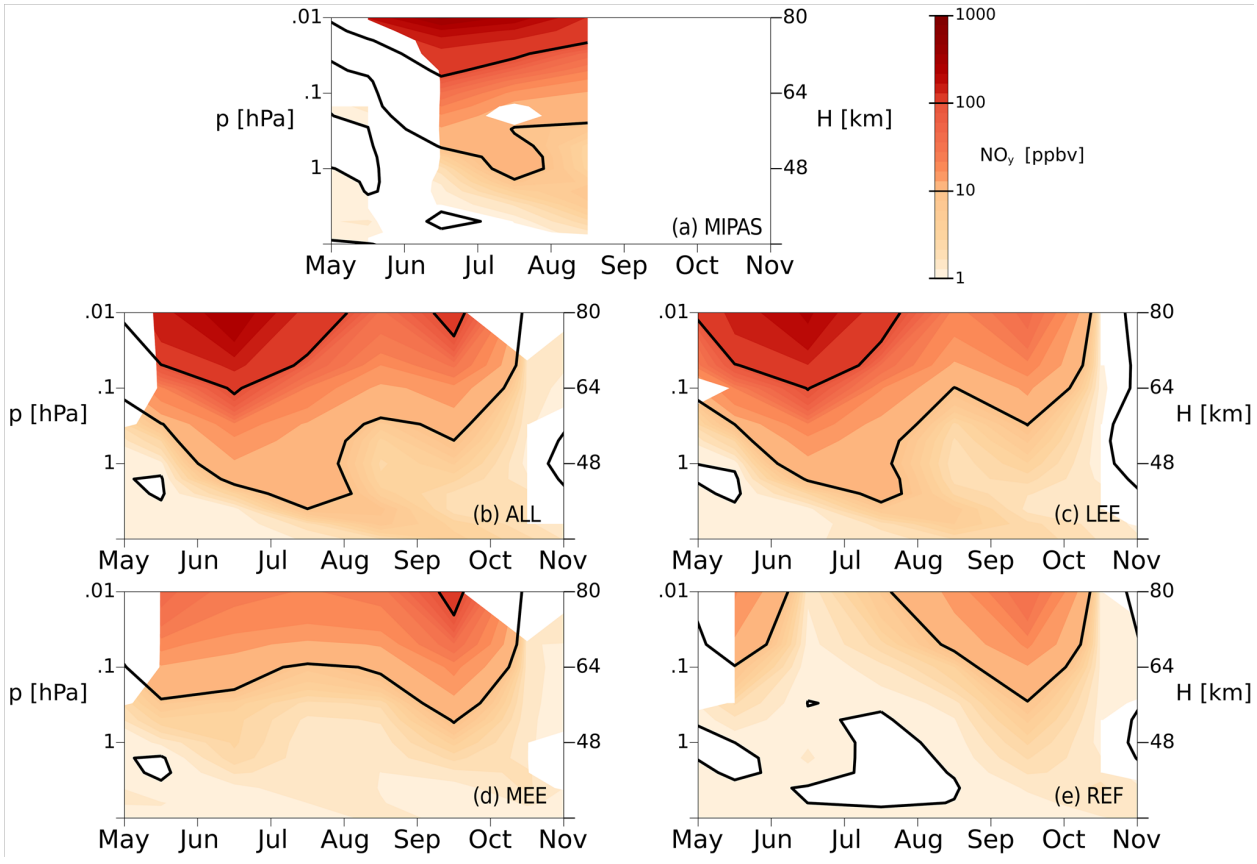

Figure 2: Monthly mean NO_y volume mixing ratio anomaly in ppbv for the Southern Hemisphere (> 70° S average) calculated as difference of the year 2005 and the average of 2006 – 2010. (a) MIPAS observations; (b) ensemble mean of ALL simulations; (c) ensemble mean of LEE simulations; (d) ensemble mean of MEE simulations; (e) ensemble mean of REF simulations. Black contour lines highlight 1, 10, 100 and 1,000 ppbv. Colored regions are significant at the 99 % confidence level (calculated using a Student t-test).

Atmos. Chem. Phys. Discuss., https://doi.org/10.5194/acp-2018-1123
Manuscript under review for journal Atmos. Chem. Phys.
Discussion started: 23 November 2018

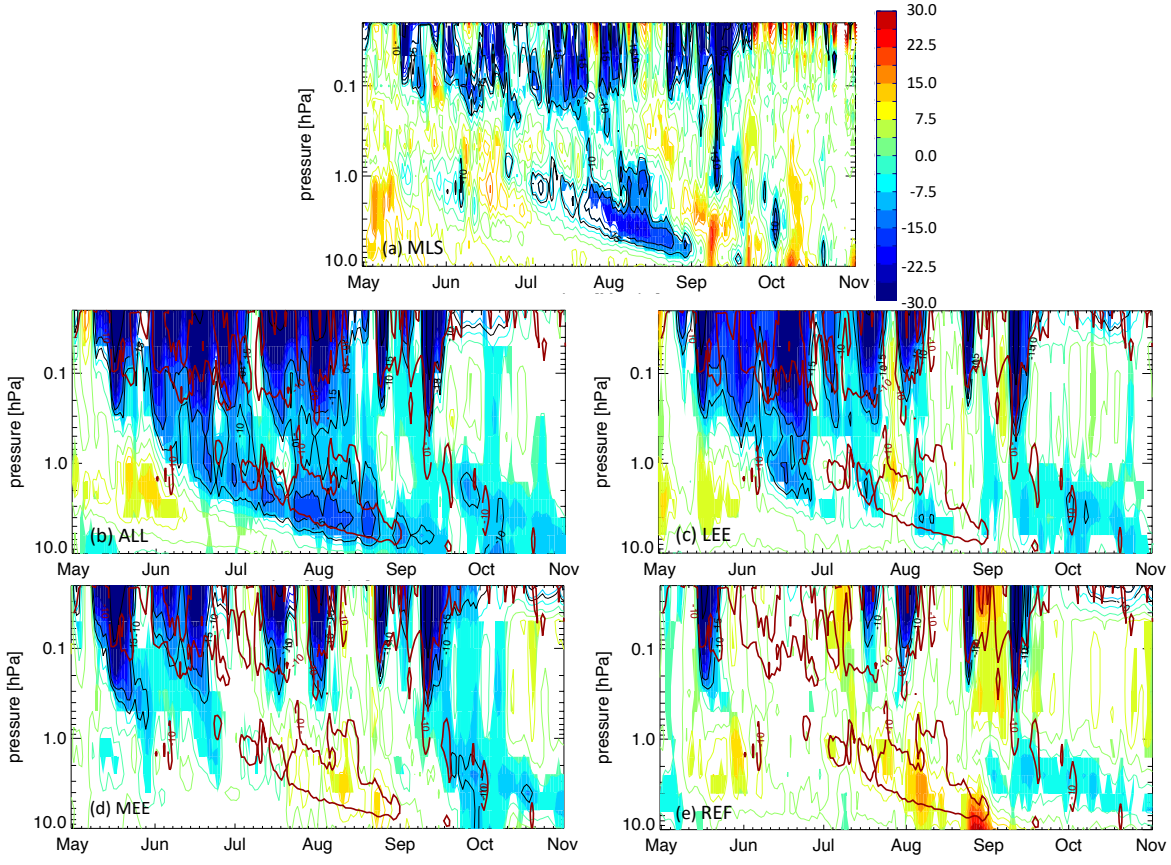

Figure 3: Monthly mean ozone anomaly poleward of 70° S calculated as difference of year 2005 and average of 2006 – 2010 relative to 2005 – 2010 period. (a) MLS observations; (b) ensemble mean of ALL simulations; (c) ensemble mean of LEE simulations; (d) ensemble mean of MEE simulations; (e) ensemble mean of REF simulations. Black lines highlight -10 %, -15% and -50 % and dark red lines mark -10 % from MLS observations on every plot. Note that mesospheric ozone depletion reaches 80-90 % during some strong solar proton events. Colored regions are significant at the 99 % confidence level (calculated using a Student t-test).

Atmos. Chem. Phys. Discuss., https://doi.org/10.5194/acp-2018-1123
Manuscript under review for journal Atmos. Chem. Phys.
Discussion started: 23 November 2018

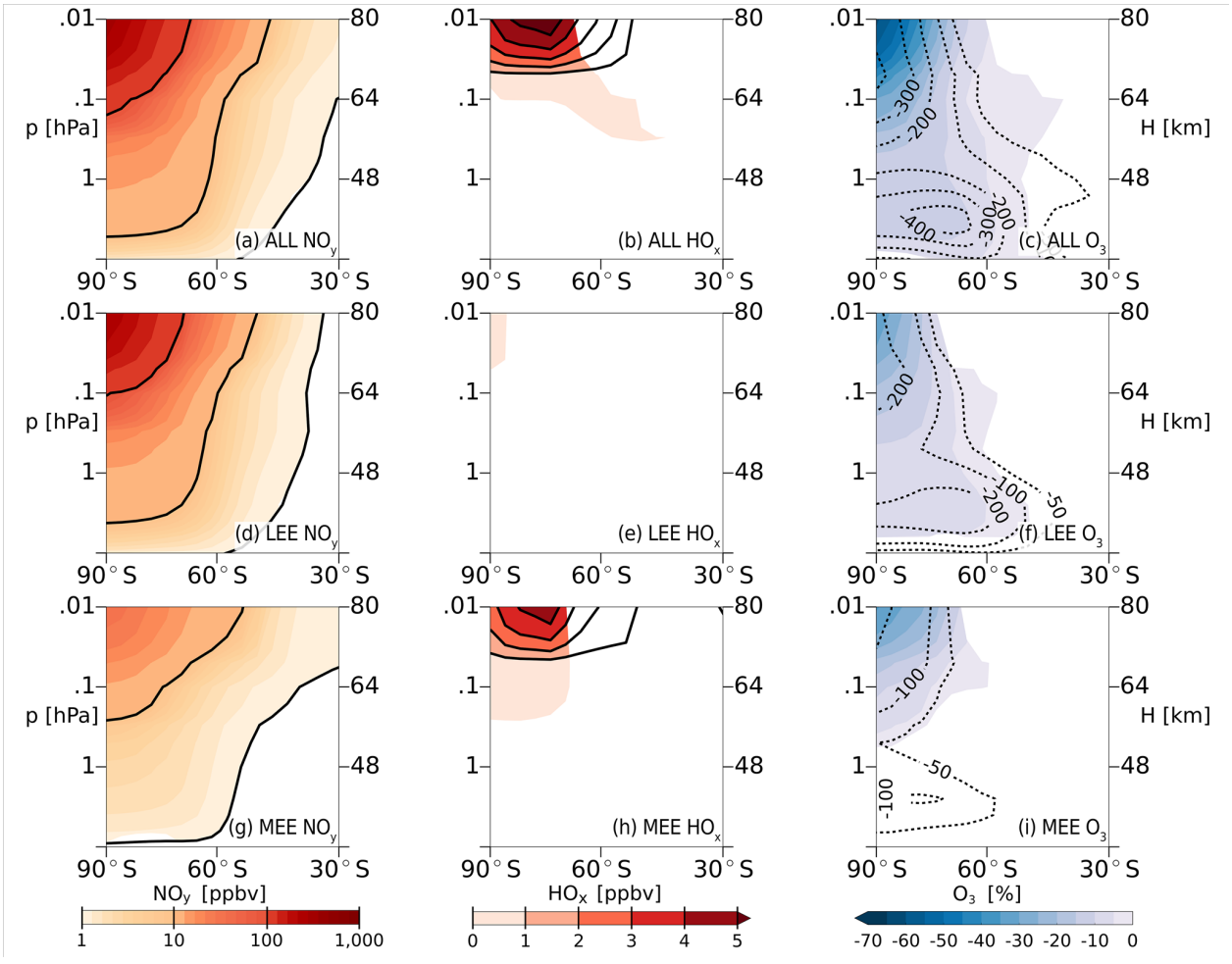

Figure 4: Summary of zonally averaged results. Columns: NO_y (left); HO_x (center); O_3 (right). Rows: including ALL energetic particles (top); only with LEE (center); only with MEE (bottom). All panels show results for the geomagnetically active period (2002 – 2005) for austral winter (JJA) from the respective simulations minus the REF simulation. Colors show absolute differences in ppbv for NO_y and HO_x plots and difference in percent for O_3 plots. Isolines show difference in absolute values in ppbv. Colored regions are significant at the 99 % confidence level (calculated using a Student t-test).